A NEW NONLINEAR THREE DIMENSIONAL FINITE ELEMENT FOR CURVED BEAMS

Bambang Suhendro[1]

ABSTRACT

*A new nonlinear geometric curved-beam finite element is developed for three dimensional space systems by using the principal of potential energy and polynomial functions. The element is assumed to be curved in one plane only, but deformations in the three-dimensional space is considered. The element geometry is defined by a second order polynomial. In deriving the linear stiffness matrix, **k**, the displacement functions are approximated by cubic polynomials. In deriving the incremental stiffness matrices, n_1 and n_2, however, while the transverse displacements are still approximated by cubic polynomials, the longitudinal displacements and twist are approximated by linear polynomials. A major improvement in the accuracy of the element is obtained by averaging the nonlinear part of the axial strain. The method of solution used is that of the fixed Lagrange coordinates and the Newton-Raphson procedure. Comparisons of numerical results with those of various other methods indicate that, in terms of the number of elements or degrees of freedom needed for convergence, the method seems significantly more effective than most. Non of the others seen to be more effective. The problems considered included shallow and deep arches, extremely thin arches, and arches of various profiles.*

1. INTRODUCTION

Many civil engineering structures such as long span arch bridges, horizontally curved highway bridges, and building frames contain curved beam elements in their main structural systems. The curved beam elements are commonly used also in aircraft, ship, and vessel frame systems. However, due to its relatively complex geometry, the analysis procedure involving curved structures is commonly done by modelling the curved part with sufficiently number of straight beam elements. Since the slope continuity of the curved beams is destroyed when several straight beam elements are introduced, this approach creates discontinuity problems at the connecting nodes, especially when it is used for nonlinear analysis. Unfortunately there are limited works in the literature that dealing with the solution of the problem. This research is conducted to develop a new generation of three-dimensional curved beam finite element that is applicable to arbitrary curved geometry and is effectively used for linear and nonlinear analyses of curved structures with high degree of accuracy.

[1] *Head of Structural Laboratory, Department of Civil Engineering, Gadjah Mada University*

A curved beam element may be characterized by its curved geometry and compressive axial strains. The latter would elicit nonlinear behavior analogous to that of a beam column even when the deformations are elastic and not necessarily large. Nonlinearity appears due to the fact that the nonlinear parts of the axial strain equation in the strain-displacement relation are kept to be considered in the formulation. It means that the effect of distortion of the structure on its response is completely taken in to account. This class of problem is known widely as geometric nonlinear problem.

Considerable work has been done on the development of suitable finite element models for the analysis of curved beams. Most of the previous works have dealt with their linear or stability analyses in the plane of the structure. Past studies that had considered out-of-plane behavior have been limited to buckling analysis formulated as an eigenvalue problem. Previous works that dealt with truly nonlinear equilibrium analysis of curved structures have been limited to behavior in the plane of the structure.

For relatively slender members, there are, in general, three approaches to represent the beam geometry: (1) straight beams, that form chords of curved segments, (2) shallow-shell or shallow-arch types of curved elements for which the Cartesian coordinate systems are used in place of the curvilinear coordinate systems, and (3) truly curved elements that use curvilinear coordinate systems.

Sufficiently number of straight-beam elements were used by Austin and Ross, among others, to obtain the buckling load of symmetrically loaded arches, while Dawe used degeneration of shallow-shell elements to analyse shallow-arch structures (Suhendro & Wen, 1991). The element geometry was represented by replacing differential length ds along the curve by the differential dx on the Cartesian x-axis that passes through the end nodes of the element. Belytschko and Glaum (1979) used higher order displacement functions for the initially curved beam element in two dimension. Accuracy is further enhanced by using a corotational formulation, a Euler-type or moving coordinate vis-a-vis the Lagrange-type or stationary coordinate system. Similar formulation also has been reported by Elias and Chen (1988).

A problem associated with nonlinear finite elements for curved beams is the so called membrane locking, i.e. excessive membrane stiffness corresponding to bending displacements. Stolarski and Belytschko (1982) showed such excess could be reduced by the strategem of reduced numerical integration. Curved-beam elements based on curvilinear coordinate system were reported by Noor and Peters (1981). A mixed formulation with independent interpolation functions for the displacements and internal forces was used. In this case, since both the nodal end forces and end displacements are used as generalized coordinates, the number of degrees of freedom per element is essentially twice that of the usual displacement formulation. However, by allowing discontinuities of forces with a condensing out of the force degrees of freedom at the element level, they showed a considerable improvements. Nonshallow circular arch analysis was also reported by Calhound and Da Deppo (1983) who used cubic polynomials for normal and tangential displacement functions. The problem was formulated as a system of rate equations that govern the quasi-static deformation of the arch. These equations were integrated using Runge-Kutta scheme to obtain load-deflection response. By means of a field transfer matrix method, Fujii and Gong (1988)

developed a curved beam element of arbritary geometry for finite displacement analisis of general planar arches. Bleeding functions of third degree were used to represent the arch geometry.

All the aforementioned works were formulated to consider arch behavior in its plane only. For three-dimentional spatial behavior, straight-beam finite elements that may be used to form chords of curved members had been employed by Wen and Rahimzadeh (1983) to study nonlinear behavior of arches. They used updated coordinates in order to deal with large displacements.

The finite element model presented herein is proposed to be a new generation of three-dimensional curved-beam finite element which is applicable to both linear and nonlinear analyses of arbritary curved geometry in two and three-dimensional space with high degree of accuracy. The element is readily incorporable for general structural engineering computer programs to make it useful for practical applications.

2. FINITE ELEMENT MODEL

Strain-Displacement Relation and Strain Energy Expression

Consider a beam element curved in one plane as shown in Fig. 1. A right handed coordinate system, *x*-, *y*-, and *z*-axes, represents the local or member coordinates of the element. The displacements corresponding to those axes are denoted by *u*, the radial displacement; *v*, the out-of-plane displacements; and *w*, the tangential displacement. The rotation about the *z*-axis is denoted by β. The centroidal axes curves in the *xz*-plane with radius of curvature *R*, which may vary. The cross section of the element is taken to be constant and has two axes of symmetry. The expression for the longitudinal strain at a point (ξ, η) in section *s*, measured along the curved centroidal axis, may be written as:

$$\varepsilon_z|_{s,\xi,\eta} = \left(\frac{dw}{ds} - \frac{u}{R}\right) + \frac{1}{2}\left(\frac{du}{ds} + \frac{w}{R}\right)^2 + \frac{1}{2}\left(\frac{dv}{ds}\right)^2 + \eta\left(\frac{\beta}{R} - \frac{d^2v}{ds^2}\right) - \xi\left[\frac{d^2u}{ds^2} + \frac{dw}{ds}\frac{1}{R} + w\frac{d}{ds}\left(\frac{1}{R}\right)\right] \quad (1)$$

in which the first term of the right-hand side = the linear axial strain; the second and the third terms = nonlinear axial strains at the centroidal axis; and the next two terms = strains due to bending.

The strain energy of the element may be written as:

$$U_E = \int_L \int_A \frac{E\varepsilon^2}{2} dA ds + \int_L \frac{GK_t}{2}\left(\frac{d\beta}{ds} + \frac{1}{R}\frac{dv}{ds}\right)^2 ds \quad (2)$$

where the first term = the strain energy due to longitudinal strain; the second term = that due to shear strain; A = the cross-sectional area; L = the length of the element; E and G =

the Young's modulus and shear modulus; and K_t = the torsional constant of the cross section.

Element Geometry

Referring to the curved element shown in Fig.2, the coordinates of the nodes A and B, with respect to the global coordinate system are (X_A,Y_A) and (X_B,Y_B), respectively. Their relative position is defined by $X_L = X_B - X_A$, and $Y_L = Y_B - Y_A$. The origin of the element local coordinate system is located at node A where the local z-axis forms an angle ϕ_A with the global X-axis. The local coordinates (X_B,Z_B) of node B are given by :

$$X_B = -X_L \sin\phi_A + Y_L \cos\phi_A \quad (3\text{-a})$$

$$Z_B = X_L \cos\phi_A + Y_L \sin\phi_A \quad (3\text{-b})$$

Let ϕ = the angle between the tangent at node A and the tangent at a given point *s*. The angle ϕ varies from zero at node A to θ at node B. The radii of curvature R at nodes A and B are denoted by R_1 and R_2, respectively. The element geometry is defined by:

$$s = b_1\phi + b_2\phi^2 \quad (4)$$

in which b_1 and b_2 are constants. The radius of curvature is:

$$R = \frac{ds}{d\phi} = b_1 + 2b_2\phi \quad (5)$$

The element length is given by

$$L = b_1\theta + b_2\theta^2 \quad (6)$$

From the boundary conditions:

$$X_B = \int_0^{X_B} dx = \int_0^{X_B} \sin\phi ds = \int_0^{\theta} R\sin\phi d\phi \quad (7\text{-a})$$

and

$$Z_B = \int_0^{Z_B} dz = \int_0^{\theta} R\cos\phi d\phi \quad (7\text{-b})$$

The resulting coefficients b_1 and b_2 are calculated as:

$$b_1 = \frac{X_B - 2b_2(\sin\theta - \theta\cos\theta)}{(1-\cos\theta)} \quad (8\text{-a})$$

$$b_2 = \frac{Z_B(1-\cos\theta) - X_B\sin\theta}{2[(1-\cos\theta)(\theta\sin\theta + \cos\theta - 1) - \sin\theta(\sin\theta - \theta\cos\theta)]} \quad (8\text{-b})$$

Thus, the geometry of the finite element as given by (4) is completely defined by X_B, Z_B, and the angle θ.

Displacement Functions

In deriving the linear stiffness matrix, the displacement functions are approximated by cubic polynomials in the normalized variables $\gamma = \phi/\theta$:

$$u = \lambda_1 + \lambda_2 \gamma + \lambda_3 \gamma^2 + \lambda_4 \gamma^3 \quad (9\text{-a})$$

$$v = \lambda_5 + \lambda_6 \gamma + \lambda_7 \gamma^2 + \lambda_8 \gamma^3 \quad (9\text{-b})$$

$$w = \lambda_9 + \lambda_{10} \gamma + \lambda_{11} \gamma^2 + \lambda_{12} \gamma^3 \quad (9\text{-c})$$

$$\beta = \lambda_{13} + \lambda_{14} \gamma + \lambda_{15} \gamma^2 + \lambda_{16} \gamma^3 \quad (9\text{-d})$$

In deriving the incremental stiffness matrices, $\mathbf{n}_1$ and $\mathbf{n}_2$, however, while the transverse displacements are still approximated by cubic polynomials, the longitudinal displacement and twist are approximated by linear polynomials only:

$$u = \alpha_1 + \alpha_2 \gamma + \alpha_3 \gamma^2 + \alpha_4 \gamma^3 \quad (10\text{-a})$$

$$v = \alpha_5 + \alpha_6 \gamma + \alpha_7 \gamma^2 + \alpha_8 \gamma^3 \quad (10\text{-b})$$

$$w = \alpha_9 + \alpha_{10} \gamma \quad (10\text{-c})$$

$$\beta = \alpha_{11} + \alpha_{12} \gamma \quad (10\text{-d})$$

As it will be shown later, the linear stiffness is obtained by using the more accurate representation of (9-a)-(9-d) and subsequently condensing out four nonessential degrees of freedom. Equations (10-a)-(10-d) are used to derive the nonlinear incremental stiffness matrices (which are functions of the displacements) in order to avoid condensation at every change of displacement values.

Element Strain Energy

The finite element, obtained by using (1) and formally following the usual potential energy formulation, was found to be too stiff. This will be illustrated by numerical results later. With a view to improving the formulation, the nonlinear terms in the strain expression are replaced by their averages over the element length. Thus, the expression for the axial strain is rewritten as:

$$\varepsilon_z|_{s,\xi,\eta} = \left(\frac{dw}{ds} - \frac{u}{R}\right) + \frac{1}{2L}\int_0^L \left(\frac{du}{ds} + \frac{w}{R}\right)^2 ds + \frac{1}{2L}\int_0^L \left(\frac{dv}{ds}\right)^2 ds \quad (11)$$

In terms of γ, the expression for the longitudinal strain can be obtained as follows:

$$\varepsilon = \left(\frac{1}{R\theta}\frac{dw}{d\gamma} - \frac{u}{R}\right) + \frac{1}{2L}\int_0^l \left(\frac{1}{R\theta}\frac{du}{d\gamma} + \frac{w}{R}\right) R\theta d\gamma + \frac{1}{2L}\int_0^l \left(\frac{1}{R\theta}\frac{dv}{d\gamma}\right)^2 R\theta d\gamma +$$

$$\eta\left[\frac{\beta}{R} - (R\theta)^{-2}\frac{d^2v}{d\gamma^2} - \frac{dv}{d\gamma}\frac{d^2\gamma}{ds^2}\right] -$$

$$\xi\left[(R\theta)^{-2}\frac{d^2u}{d\gamma^2} + \frac{du}{d\gamma}\frac{d^2\gamma}{ds^2} + R^{-2}\theta^{-1}\frac{dw}{d\gamma} + \frac{w}{R}\frac{d^2\gamma}{dsd\gamma}\right] \qquad (12)$$

in which : $\frac{d\gamma}{ds} = \frac{1}{R\theta}; \frac{d^2\gamma}{ds^2} = -\frac{1}{R^3\theta^3}\frac{dR}{d\gamma}; \frac{d^2\gamma}{dsd\gamma} = R\theta\frac{d^2\gamma}{ds^2}$ (13)

By use of equations (2) and (12), the strain energy of the element can be written as:

$$U_E = U_2 + U_3 + U_4 \qquad (14)$$

in which U_2, U_3, and U_4, containing the quadratic, cubic, and quartic terms, respectively, of the displacement field variables, are given by:

$$U_2 = \frac{E}{2}\int_0^l \left[\frac{A}{R\theta}\left(\frac{dw}{d\gamma} - \theta u\right)^2 + I_\xi\frac{\theta}{R^3}\left(R\beta - \theta^{-2}\frac{d^2v}{d\gamma^2} - R^2\frac{dv}{d\gamma}\frac{d^2\gamma}{ds^2}\right)^2 +\right.$$

$$\left.\frac{I_\eta}{R^3\theta^3}\left(\frac{d^2u}{d\gamma^2} + \frac{du}{d\gamma}\frac{d^2\gamma}{ds^2}R^2\theta^2 + \frac{dw}{d\gamma}\theta + w\frac{d^2\gamma}{dsd\gamma}R\theta^2\right)^2 - \right] d\gamma +$$

$$\frac{GK_t}{2}\int_0^l \frac{1}{R^3\theta}\left(R\frac{d\beta}{d\gamma} + \frac{dv}{d\gamma}\right)^2 d\gamma \qquad (15)$$

$$U_3 = EA\int_0^l \left(\frac{dw}{d\gamma} - \theta u\right) M d\gamma \qquad (16)$$

$$U_4 = \frac{EA}{2}\int_0^l R\theta (M)^2 d\gamma \qquad (17)$$

where $I_\xi = \int_A \eta^2\, dA$, and $I_\eta = \int_A \xi^2\, dA$, are the moments of inertia of the cross section about ξ– and η–axes respectively, and

$$M = \frac{1}{2L}\int_0^l \left[\left(\frac{1}{R\theta}\frac{du}{d\gamma} + \frac{w}{R}\right)^2 + \left(\frac{1}{R\theta}\frac{dv}{d\gamma}\right)^2\right] R\theta d\gamma \qquad (18)$$

It represents the average of the nonlinear part of the axial strain.

Linear Stiffness Matrix

As mentioned previously, in deriving the linear stiffness matrix, the displacement functions are approximated by cubic polynomials given in equations (9-a)-(9-d). Upon substituting those equations into equation (15), U_2 becomes a function of the coefficients λ_i in the displacement functions. By use of the boundary conditions at the end nodes, these coefficients may be replaced by the nodal degrees of freedom. They consist of the essential degrees of freedom: u_A and u_B = the radial displacements; v_A and v_B = the transverse displacements; w_A and w_B = the longitudinal displacements; β_A and β_B = the twists about the longitudinal axis; θ_{yA} and θ_{yB} = $(du/ds + w/R)_{A \text{ or } B}$ = the rotations about y-axis; θ_{xA} and θ_{xB} = $(-dv/ds)_{A \text{ or } B}$ = the rotations about x-axis; and the nonessential degrees of freedom: $(dw/ds)_A$, $(dw/ds)_B$, $(d\beta/ds)_A$, and $(d\beta/ds)_B$. They will be denoted collectively by a vector q. Thus, U_2 can be written as:

$$U_2 = \int_0^1 f_2(q)d\gamma \tag{19}$$

in which f_2 = a quadratic function of the q's.

The linear stiffness matrix, **k**, may be obtained as

$$\mathbf{k} = (k_{ij}) = \left(\frac{\partial^2 U_2}{\partial q_i \partial q_j}\right) = \left(\int_0^1 \frac{\partial^2 f_2}{\partial q_i \partial q_j} \partial\gamma\right) \tag{20}$$

The expressions for the integrand in terms of the q's in equation (20) have been explicitly discussed by Suhendro (1994). After condensing out the aforementioned nonessential degrees of freedom, the resulting 12x12 linear stiffness matrix has then the same size as the incremental stiffness matrices that are developed in the following.

Incremental Stiffness Matrices

The incremental stiffness matrices, $\mathbf{n}_1$ and $\mathbf{n}_2$, are derived by first substituting equations (10-a)-(10-d) into equations (16) and (17). The coefficients α_i are then replaced by the previously defined 12 essential degrees of freedom, which will be denoted collectively by vector *p*. Thus, U_3 and U_4 can be written as:

$$U_3 = \int_0^1 f_3(p)d\gamma \tag{21}$$

$$U_4 = \int_0^1 f_4(p)d\gamma \tag{22}$$

in which f_3 and f_4 = cubic and quartic functions of *p*, respectively.

The incremental stiffness matrices, $\mathbf{n}_1$ and $\mathbf{n}_2$, may be calculated from:

$$n_1 = (n_{1,ij}) = \left(\frac{\partial^2 U_3}{\partial p_i \partial p_j}\right) = \left(\int_0^1 \frac{\partial^2 f_3}{\partial p_i \partial p_j} \partial\gamma\right) \tag{23}$$

$$n_2 = (n_{2,ij}) = \left(\frac{\partial^2 U_4}{\partial p_i \partial p_j}\right) = \left(\int_0^1 \frac{\partial^2 f_4}{\partial p_i \partial p_j} \partial\gamma\right) \tag{24}$$

The expressions in closed form for the elements of these matrices are available upon request to the author.

System Equilibrium Equations

The structural linear stiffness matrix **K** and incremental stiffness matrices **N1** and **N2** can be assembled from the corresponding element matrices in the usual fashion of finite element analysis via the displacement method. The potential energy of the system may be written as:

$$\Pi = \lfloor Q \rfloor \left(\frac{1}{2}[K] + \frac{1}{6}[N1] + \frac{1}{12}[N2]\right)\{Q\} - \lfloor Q \rfloor \{P\} \tag{25}$$

in which Q = the row vector of the degrees of freedom of the structure, and P = the load vector corresponding to Q. The first variation of the potential energy produces the equilibrium equation:

$$\left([K] + \frac{1}{2}[N1] + \frac{1}{3}[N2]\right)\{Q\} = \{P\} \tag{26}$$

The term in the parentheses defines the **secant stiffness matrix.**

The equations governing the linear incremental behavior follow from the second variation of the potential energy and are given by:

$$\left([K] + [N1] + [N2]\right)_{\{Q^*\}} \{\Delta Q\} = \{\Delta P\} \tag{27}$$

in which $\{Q^*\}$ denotes the displacements at a reference equilibrium position; and ΔQ and ΔP = the incremental displacement and load vectors, respectively. The term in the parentheses defines the **tangent stiffness matrix.**

3. NUMERICAL SOLUTION STRATEGY

The nonlinear load-displacement relations were calculated by use of Newton-Raphson method. It is a second order iterative method using the tangent stiffness. The load is applied as a series of small increments. For each increment an iteration scheme is employed to continuously update the tangent stiffness matrix as improved approximations of the incremental deformations are calculated. The convergence check is

based on the unbalanced force vector, which is evaluated by use of secant stiffness. A convergence tolerance of 1% of the load increment was used.

A computer program NONCURVE, which stands for Nonlinear Analysis of Curved Beam Structures, implementing the solution procedures discussed herein has been developed, and a number of numerical examples are considered to demonstrate the effectivity and accuracy of the proposed new element.

4. NUMERICAL RESULTS

A number of numerical examples of inplane and out-of-plane nonlinear behavior of arches are considered. Various types of loading, support condition, arch type (shallow and deep), and arch geometry (circular, semi-elliptic, parabolic, and sinusoidal) have been covered. The first ten examples deal with two-dimensional, inplane behavior, while the next two examples illustrates out-of-plane response to an increasing inplane loading. All resulting nonlinear load-displacement responses have been compared to the available nonlinear solutions solved by previous researchers using completely different models, and been compared also to their buckling loads obtained by other researchers based on the solution of eigenvalue problem, whenever available.

Comparison of averaged strain and unaveraged strain solutions

Comparison of numerical results corresponding to the averaged nonlinear axial strain model and the unaveraged nonlinear axial strain model as described in the following numerical results show that the unaveraged strain model is too stiff.

The difference in the behavior of the models is due to the following. The incremental stiffness matrices n_1 and n_2 may be regarded as corrections to the linear stiffness. The matrix n_1 does not differ much between the two models. When the axial strains are compressive, it tends to decrease the stiffness, and generally overdoes it. The matrix n_2 tends to make up for this by increasing the stiffness. For the unaveraged strain model, it substantially overshoots, i.e., making the model too stiff. It could be shown that the averaging process reduces the strain energy, resulting in a more flexible and more accurate model.

A 90^0-hinged circular arch subjected to uniform radial load

The geometry, physical properties and loading condition for this problem are shown in Figure 3. It is well known that this type of problem has a buckling mode which is antisymmetry or exhibits sidesway. In order to obtain such mode, a small horizontal perturbing load equal to 1% of P applied at the crown in +X direction has been introduced.

The resulting load-displacement curves for different number of elements are depicted in Figure 3. The results were obtained with a load increment (Δq) of 3.395 and an unbalanced force tolerance ε = 1% of the load increment. Different load increments were also used to solve the problem. It was observed that the results were not sensitive to the load increment used. However, near the critical load level, where the

displacements increases rapidly, smaller load increments are needed to get enough data points for drawing the load-displacement curve. It can be seen from Figure 3 that the left quarter point gradually deflects inward until buckling occurs, while the right quarter point initially deflects inward and when the intensity of the applied load is about 2/3 of the critical load it deflects outward until buckling takes place. Thus the final modes is antisymmetric. As expected, the critical load obtained from nonlinear analysis agrees very well with that obtained from eigenvalue solution reported by Wen and Lange (1981).

A hinged parabolic arch subjected to uniform load on horizontal projection

The problem considered is illustrated in Figure 4. As before, in order to obtain an antisymmetrical buckling mode, a small horizontal perturbing load equal to 1% of P (P=56.25 q) was applied at the crown in +X direction.

The resulting load-displacement curves for different number of elements are shown in Figure 4. The results were obtained with a load increment of 200 (equivalent to q=3.556) and an unbalanced force tolerance ε = 1% of the load increment. The left quarter point gradually deflects inward until buckling occurs, while the right one initially deflects inward. When the applied load intensity is about 84% of the critical load it deflects outward until buckling takes place. The critical load obtained agrees very well with that of analytical value discussed in Timoshenko's book.

A 28^0-clamped circular arch subjected to a vertical concentrated load at crown

The problem considered is illustrated in Figure 5. The load-displacement curves shown in the figure were obtained with a load increment of 2000 and ε = 0.5% of the load increment. The loading was continued until the apex had displaced an amount equal to approximately 1.5 times the initial rise of the arch. Different numbers of element, i.e.: 2, 4, and 8, to represent the one half of the arch were considered.

It can be seen in Figure 5 that even when only two elements were used, the resulting load-displacement curve was close enough to that obtained by Belytschko and Gaum (1979) with 10 elements, as well as the analytical solution. Figure 5 also shows the resulting load-displacement curves obtained by Belytschko and Gaum with 2 and 5 elements, which are less accurate than that obtained by the proposed method.

A 60^0-clamped circular arch subjected to a vertical concentrated load at crown

The problem is illustrated in Figure 6. It was solved with a load increment of 50 and ε = 1% of the load increment. Different number of elements, i.e.: 2, 4, 8, and 16, to represent the one half of the arch were considered. The results are given in Figure 6. As shown in the figure, the resulting load-displacement curves for 4, 8, and 16 elements have no significant differences. Those curves agree very well with that of obtained by Calhoun and DaDeppo (1983). The critical load obtained and the corresponding crown displacement also agree very well with those obtained analitically by DaDeppo and Schmidt, as well as by Austin and Ross who used 24 elements for their eigensolution (Suhendro & Wen, 1991).

A clamped multiple radii circular arch subjected to a vertical concentrated load at crown

This problem demonstrates the extended capability of the proposed method and the computer program for solving an arbitary arch profile. The arch has two different radii, R_1=200 and R_2=100. The two radii have a common tangent point at the crown of the arch. A vertical concentrated load is applied at the crown, as shown in Figure 7. Since the geometry is not symmetry, the entire arch should be considered. Two different numbers of element, i.e.: 4 and 8, were used to solve the problem. A load increment of 50 and a tolerance of 2% of the load increment were used. The resulting load- displacement curves are shown in Figure 7. Both curves agree well with that obtained by Calhoun and DaDeppo (1983). The resulting buckling mode is symmetric, and the maximum deflection is of the order of 7% of the arch span.

A clamped semi-circular arch subjected to a vertical concentrated load at crown

The problem is illustrated in Figure 8. Two thickness ratios of the arch were considered, namely h/R=0.05 and 0.005. The problem was solved by the proposed method with a load increment of 0.384 EI/R^2. The resulting load-displacement curves for 3, 4, and 8 elements (equivalent to 7, 10, and 22 degrees of freedom, respectively) representing the one half of the arch are shown in Figure 8. The results agree very well with that obtained by using 6 elements (equivalent to 37 degrees of freedom) of Noor et al (1977) based on a mixed formulation of finite element. The order of the displacement is approximately 20% of the arch span.

Arches with different profiles

To provide further comparisons of results with existing solutions, arches with semi-elliptic, circular, parabolic, and sinusoidal profiles having the same rise to span ratio, span, and cross-sectional properties were considered. All arches are hinged supported at their both ends and are subjected to a concentrated vertical load at crown. The symmetrical buckling of those arches were analysed by different numbers of element. All problems were solved with a load increment of 100 and an unbalanced force tolerance ε = 1% of the load increment.

Figure 9 shows the load-displacement curves obtained by the proposed method using different numbers of elements. For the sinusoidal arch, four elements of the proposed model give results comparable to those for 20 elements of Fujii and Gong (1988). For the parabolic and circular arches, results using two elements of the proposed model are close to those for 20 elements of Fujii and Gong (1988). The two elements circular arch solution is also close to Huddleston's analytical solution. For the semi-elliptic arch, four elements (11 degrees of freedom) of the proposed model give results comparable to those for six elements (38 degrees of freedom) in Noor et al. (1987) and for eight straight beam elements using the model in Wen and Rahimzadeh (1993).

Out-of plane behavior

While the preceeding numerical examples all treat in-plane response, this example considers out-of-plane response involving torsion as well as biaxial bending. The parabolic arch shown in Figure 10 is subjected to a uniform vertical load and a small (perturbing) concentrated lateral load at the crown equal to 0.000125 x total vertical load. The structure is restrained at the supports against all translations and rotations about x- and z-axis, but not about the y-axis. The load-displacement behavior indicates an ultimate vertical load that is quite close to the lateral buckling load as given in Wen and Lange (1981) via an eigenvalue solution.

Another out-of-plane problem illustrated in Figure 11 has been considered. The 90^0-hinged circular arch subjected to uniform radial load shown in Figure 11 has an out-of-plane buckling mode which is symmetric. To obtain such mode, a small lateral perturbing load equal to 0.1% of **P** applied at the crown in +z direction was introduced. In this case the rotation degrees of freedom about the x- and z-axis at the supports were restrained. Because of the symmetry of the geometry, loading, and buckling mode, only one half of the arch needs be considered. The resulting load-displacement curves for different number of elements asymptotically approaches the buckling load of the arch obtained numerically by Wen and Lange (1981) based on eigenvalue solution.

5. DICUSSION

Comparison with previous works

Previous comparisons, as given in Figures 3, 4, 5, 6, 7, 8, 9, 10, and 11, indicate that the proposed "averaged axial strain model" compete very well with the other models. In terms of the number of elements needed for accurate results, the preceding comparisons show that the proposed method is more effective than the others.

Approaches of nonlinear elastic analysis

It is generally known that curved beam elements has the tendency to be too stiff unless the in-plane displacement field is represented by sufficiently high order polynomials. This phenomenon is called as membrane locking. To overcome this problem, four approaches have been suggested: (a) to use higher order polynomials for the displacement field, as suggested by Dawe; (b) to use a mixed formulation of the finite element as in the work of Noor et al; (c) to use reduced integration technique as suggested by Stolarski and Belytschko; and (d) to use average axial strain model, as described herein.

Using higher order (e.g.: quintic) polynomials in a nonlinear analysis would involve a large amount of work with no guarantee of success. Perhaps, that is the reason why it had not been tried thus far. Using a mixed formulation, since both nodal displacements and forces are considered as degrees of freedom, matrices of larger size are involved and the formulation is inconvenient for inclusion in a general structures program. Using reduced integration technique, since the numerical integration is carried out by using only 1 or 2 Gauss points, there is a "mathematical looseness" or computational artificiality

involved, which does not appear desirable. Furthermore, the possibility of existence of zero energy mode should be of concern.

The present study indicates that the proposed average axial strain model overcomes all the above difficulties. The procedure is simpler and more efficient than the other approaches, the integration is carried out as it should be, and the accuracy of the results is generally better.

Nature of $[n_1]$ and $[n_2]$ matrices

The reason why the averaged axial strain model produces more accurate results than the unaveraged axial strain model appears to be the fact that the averaging process reduces the strain energy and thus decreases the stiffness to the correct order of magnitude. Both averaged and unaveraged axial strain models produce an identical linear stiffness matrix [k], however, the nonlinear incremental stiffness matrices $[n_1]$ and $[n_2]$ are different.

As discussed previously, the incremental stiffness matrices $[n_1]$ and $[n_2]$ may be regarded as corrections to the linear stiffness. The matrix $[n_1]$ does not differ much between the two models. When the axial strains are compressive, it tends to decrease the stiffness, and generally overdoes it. The matrix $[n_2]$ tends to make up for this by increasing the stiffness to the correct order of magnitude. For the unaveraged strain model, it substantially overshoots, i.e., making the model too stiff.

6. CONCLUSIONS

In this study, a three dimensional nonlinear curved beam element has been developed. It has 12 degrees of freedom in 6 displacements (all "essential") per node. The resulting incremental stiffness matrices $[n_1]$ and $[n_2]$, which are linear and quadratic functions of the displacements, respectively, could be expressed in closed form. Thus it can readily be incorporated into a general structural computer program.

The element, which is formulated based on the average axial strain model, is shown to be more effective and more accurate than all methods compared. The reason why the averaged axial strain model produces more accurate results appears to be the fact that the averaging process reduces the strain energy and thus decreases the stiffness to the correct order of magnitude. The method, which is based on the fixed Lagrangian coordinate system, works very well for problems involving displacements up to approximately 25% of the arch span. Not having to update the coordinates, the method saves the computational effort needed for that purpose. The fixed-coordinates approach and an explicit secant stiffness assure that the force-total displacement relationship is unique, which can be an important consideration in problems involving many cycles of loading and unloading.

The present study is limited to geometric nonlinearity. For many practical problems, when geometric nonlinearity becomes significant, effects of material nonline-arity would become important at the same time. Thus, future studies of nonlinear analysis of curved beam structures should include these effects.

7. REFERENCES

Calhoun, P.R., DaDeppo, D.A., 1983, Nonlinear Finite Element Analysis of Clamped Arches, *Journal of Structural Engineering, ASCE*, Vol.109, No.3, pp.599-612.

Elias, Z.M., Chen, K.L., 1988, Nonlinear Shallow Curved-Beam Element, *Journal of Engineering Mechanics, ASCE*, Vol.114, No.6, pp.1076-1087.

Fujii, F., Gong, S., 1988, Field Transfer Matrix for Nonlinear Curved Beams, *Journal of Structural Engineering, ASCE*, Vol.114, No.3, pp.675-691.

Noor, A.K., Peters, J.M., 1981, Mixed Models and Reduced/Selective Integration Displacement Models for Nonlinear Analysis of Curved Beams, *International Journal of Numerical Methods Engineering*, Vol.17, No.4, pp.615-631.

Stolarski, H., Belytschko, T., 1982, Membrane Locking and Reduced Integration for Curved Elements. *Journal of Applied Mechanics, ASME*, Vol.49, No.1, pp.172-176.

Suhendro, B., Wen, R.K., 1991, Nonlinear Finite Element for Curved Beams, *Journal of Structural Engineering, ASCE*, Vol.117, No.11, pp.3496-3515.

Suhendro, B., 1994, Finite Element Model for Linear Three Dimensional Analysis of Arch Structures, *Proceedings of the Finite Element Method Seminars*, ITB-Bandung, Dec.15-16, pp.41-55.

Suhendro, B., 1996, Buckling Analysis of Structures by Finite Element Method, *Proceedings of the Finite Element Method Seminars*, ITB-Bandung, Dec.19-20, pp.151-156.

Wen, R.K., Rahimzadeh, J., 1983, Nonlinear Elastic Frame Analysis by Finite Element, *Journal of Structural Engineering, ASCE*, Vol.109, No.8, pp.1952-1971.

Wen, R.K., Lange, J.G., 1981, Curved Beam Element for Arch Buckling Analysis, *Journal of Structural Engineering, ASCE*, Vol.107, No.11, pp.2053-2069.

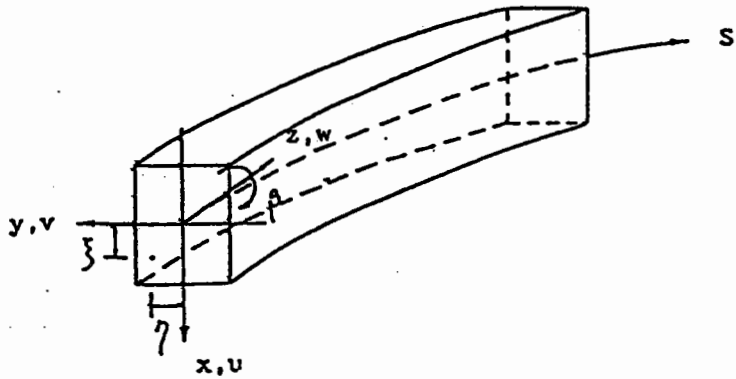

Figure 1. Curved beam element

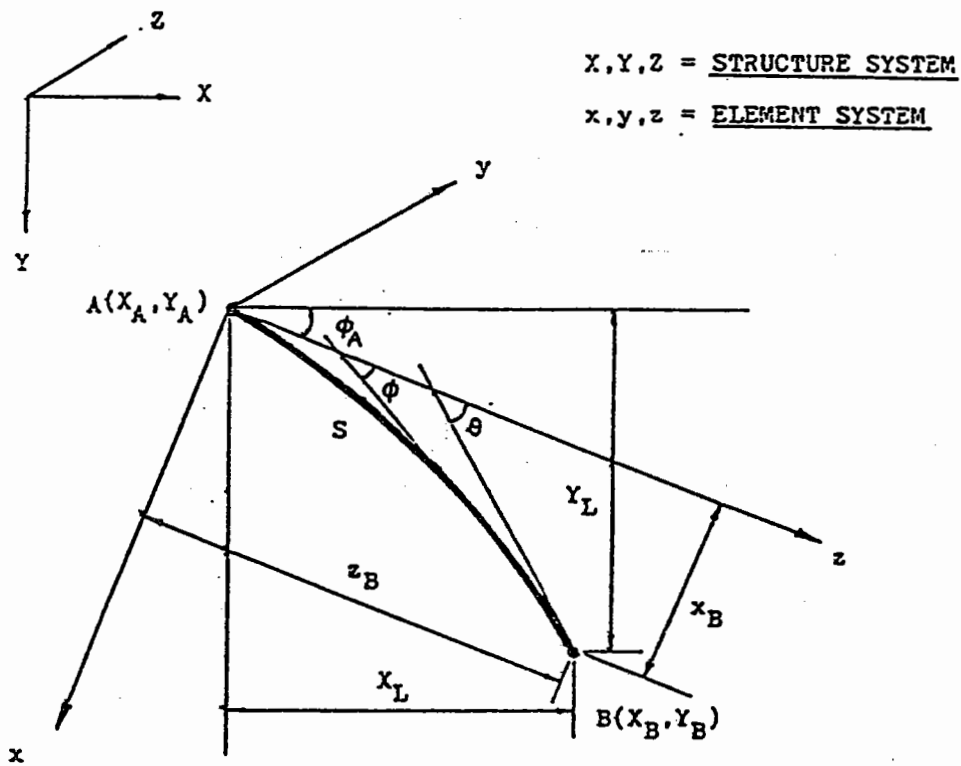

Figure 2. Curvilinear coordinate systems

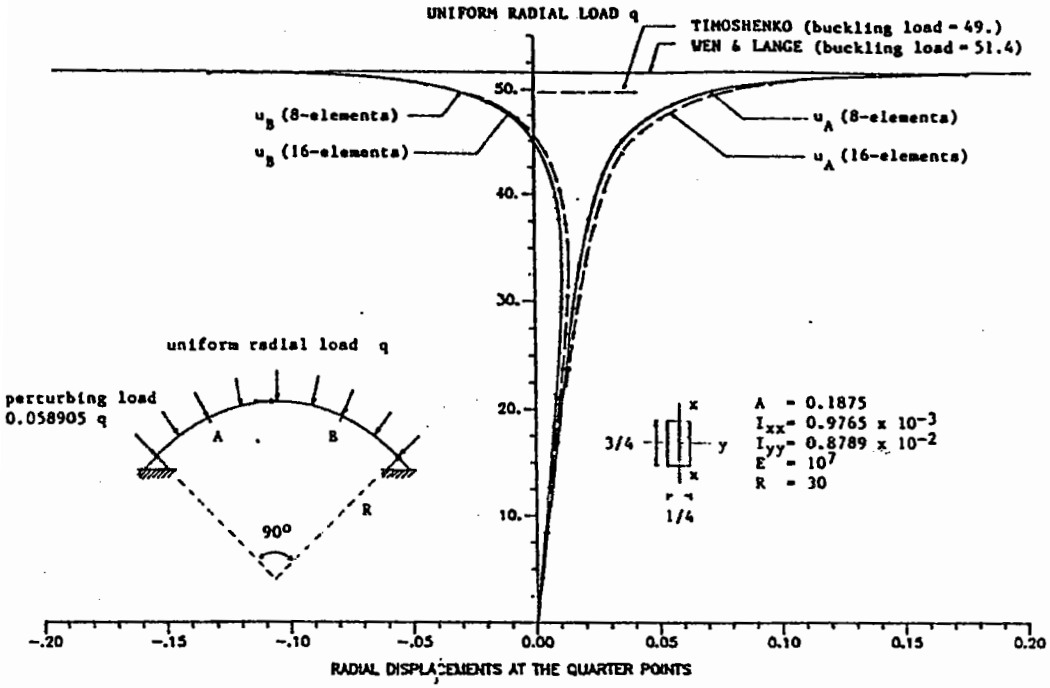

Figure 3. A 90° hinged circular arch subjected to uniform radial load

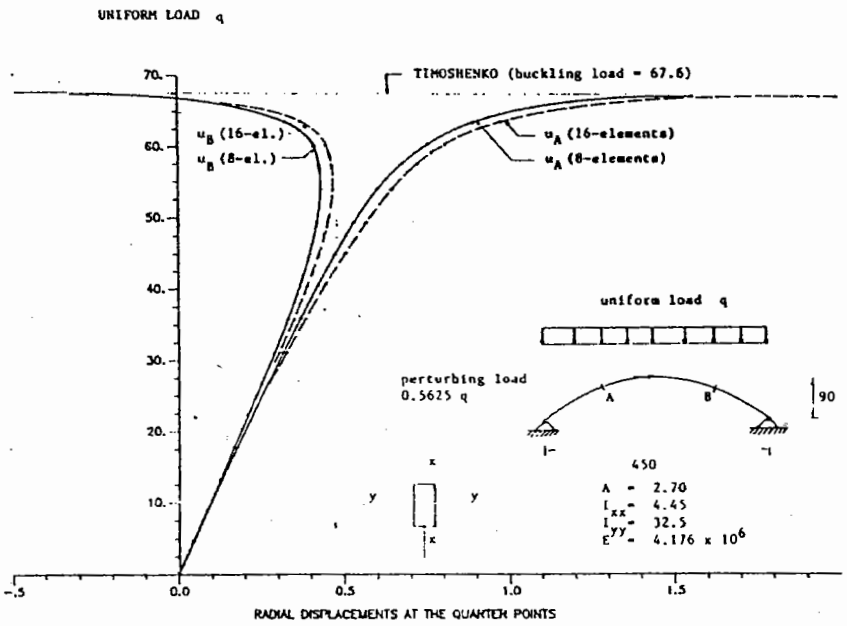

Figure 4. A hinged parabolic arch subjected to uniform load on horizontal projection

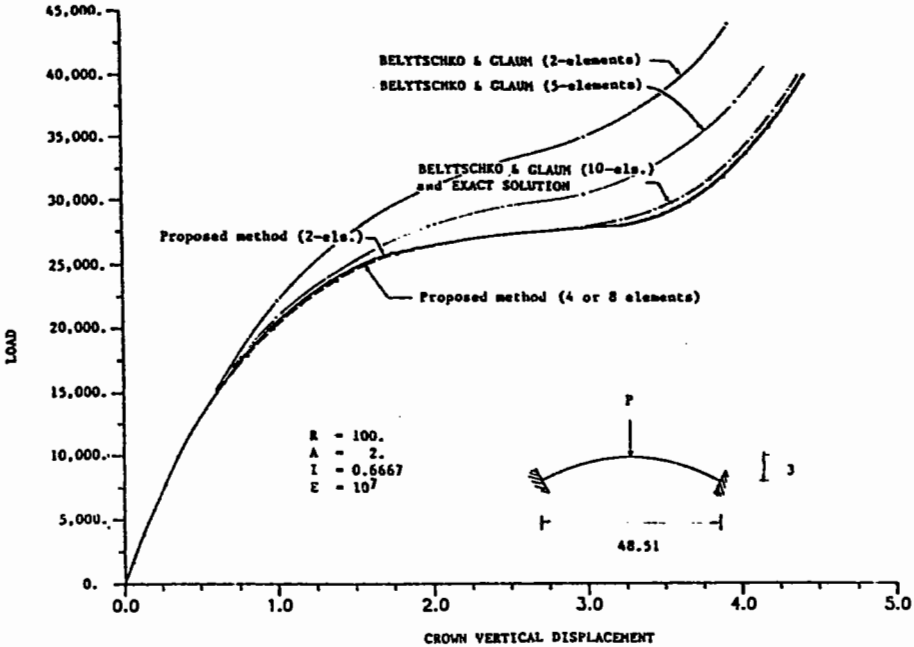

Figure 5. A 28° clamped circular arch subjected to a vertical concentrated load at crown

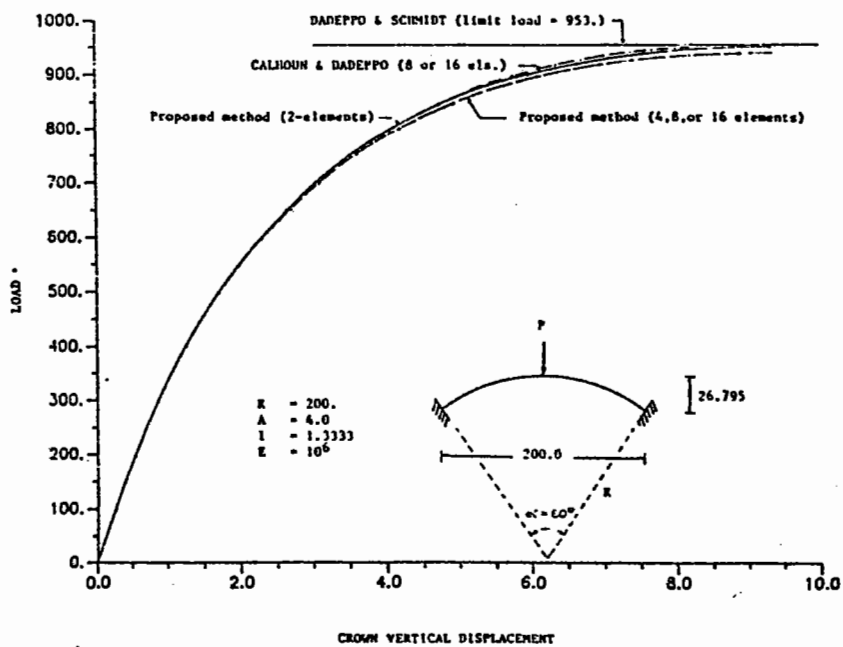

Figure 6. A 60° clamped circular arch subjected to a skew concentrated load at crown

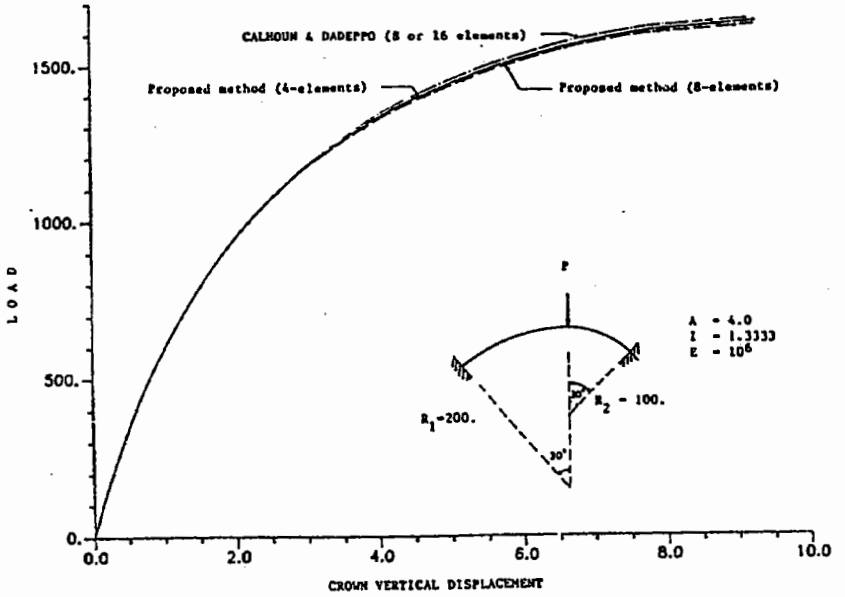

Figure 7. A clamped multiple radii circular arch subjected to a vertical concentrated load at crown

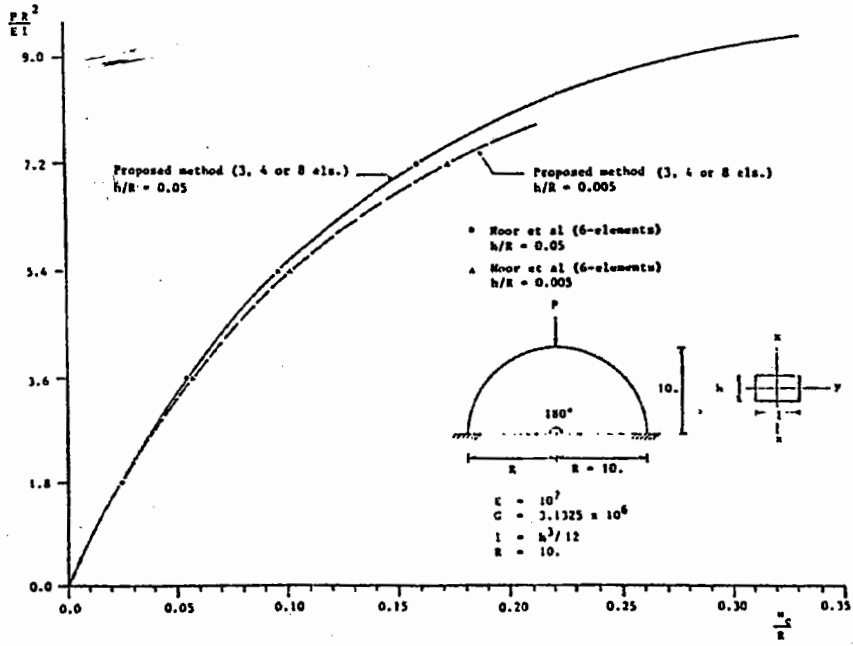

Figure 8. A clamped semi-circular arch subjected to a vertical concentrated load at crown

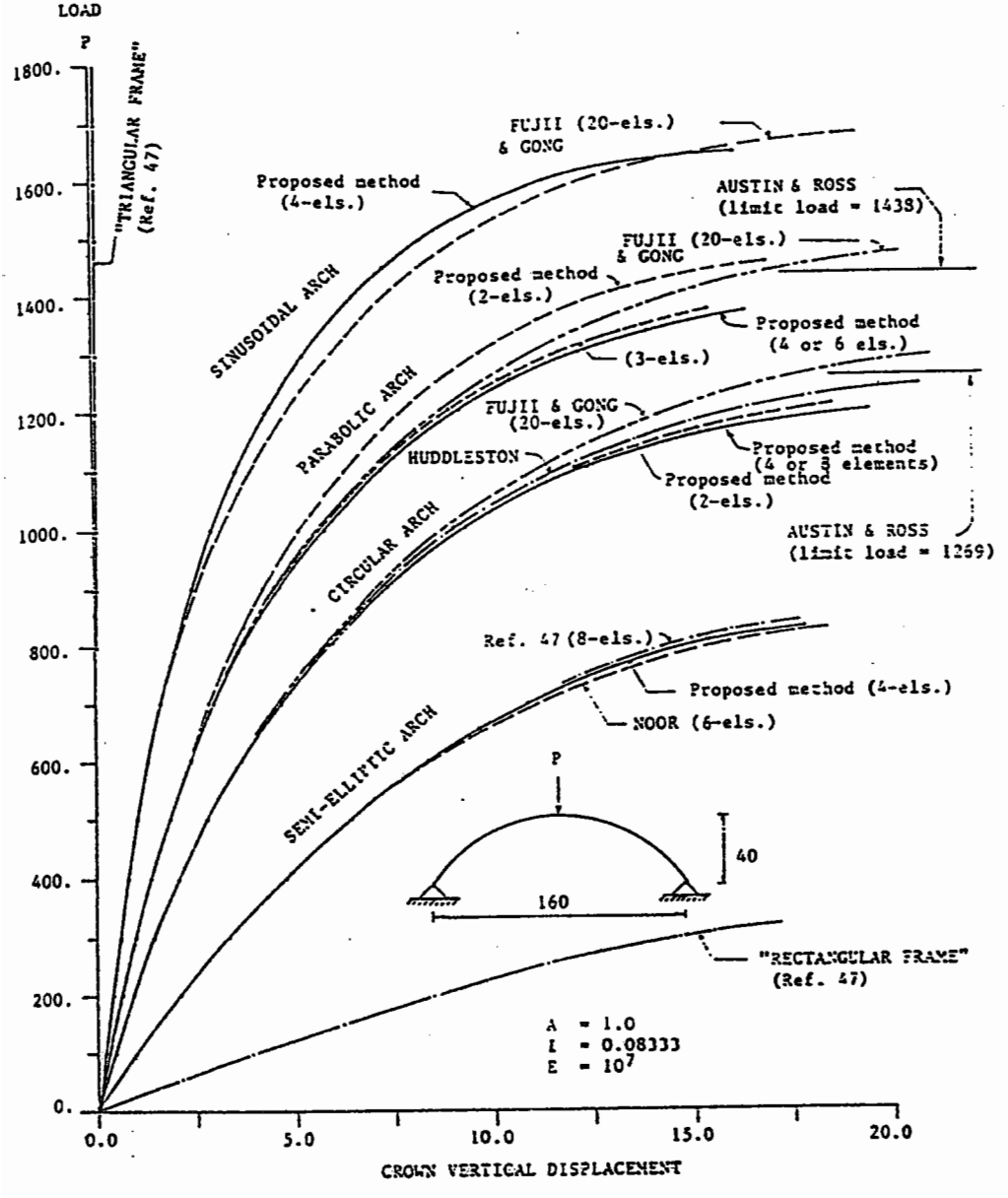

Figure 9. Sinusoidal, parabolic, circular, semi-elliptic arches subjectec to a concentrated load at their crowns

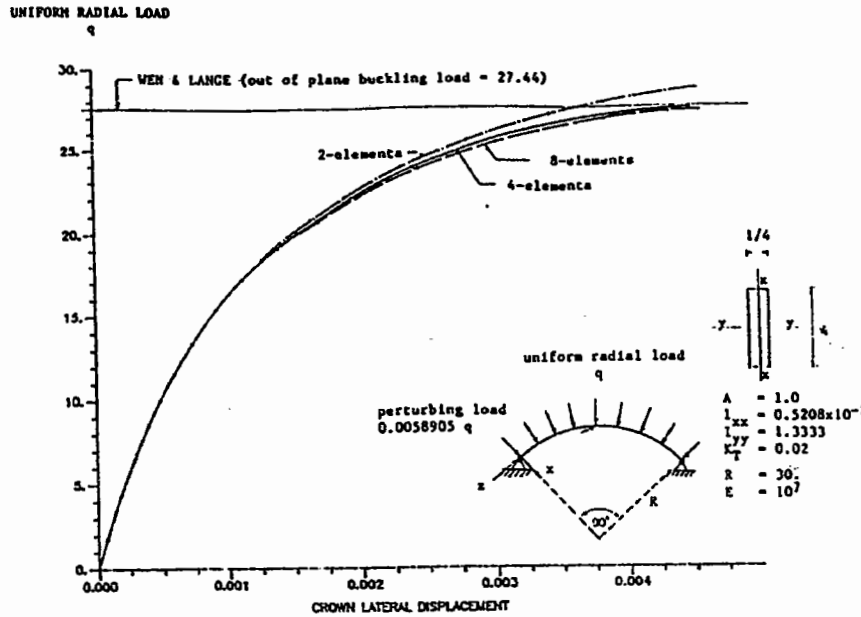

Figure 10. A hinged parabolic arch subjected to uniform load on horizontal projection (out-of-plane behavior)

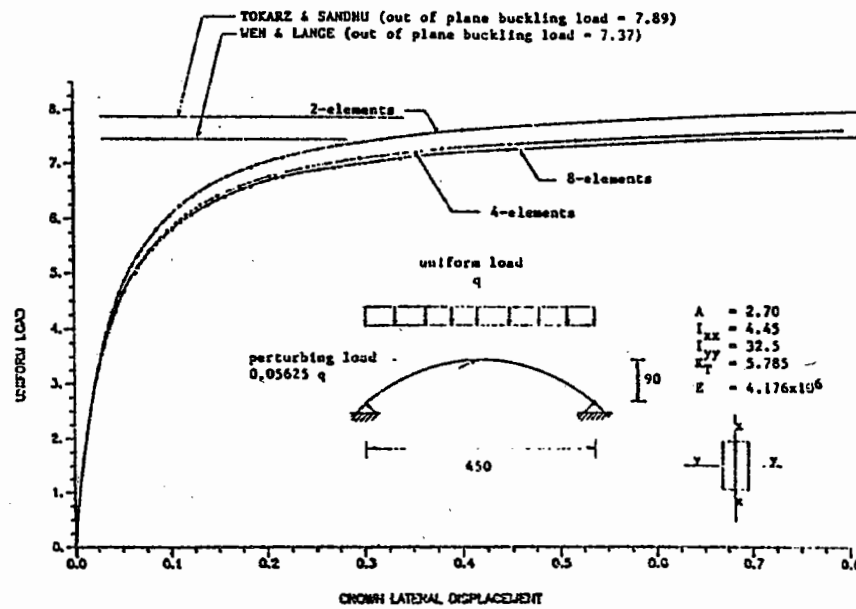

Figure 11. A 90° hinged circular arch subjected to uniform radial load (out-of-plane behavior)